Ka-/*K*-Band Frequency-Reconfigurable Single-Input Differential-Output Low-Noise Amplifier for 5G Applications

Hao-Hsuan Chen and Zuo-Min Tsai, *Senior Member, IEEE*

***Abstract*— This letter describes the design, analysis, and performance measurements of a *Ka*- and *K*-band frequency-reconfigurable single-input differential-output (SIDO) low-noise amplifier (LNA) with a compact core size of 0.157 mm^2. At 28 and 39 GHz, respectively, the noise figures of the LNA were 2.8 and 4.4 dB; it had high differential gains of 20.1 and 14.9 dB. The proposed LNA was fabricated using the 65-nm CMOS process. The LNA includes a two-stage common-source (CS) buffer amplifier to achieve low noise and an active balun for converting single-ended signals into differential signals. Moreover, a substrate-shield-based inductor and tunable matching networks were used to achieve the frequency reconfiguration function of the LNA. The gain and phase imbalances were 0.3 and 0.2 dB, and 5.4° and 6° at 28 and 39 GHz, respectively. Compared with published multiband SIDO LNAs, the proposed amplifier achieved higher figures of merit (FoMs) of 3.52 and 1.77 while maintaining a compact core size. Therefore, the LNA is suitable for *K*- and *Ka*-band 5G communication applications.**

***Index Terms*— CMOS, low-noise amplifier (LNA), monolithic microwave integrated circuit, multiband, single-input differential-output (SIDO), substrate-shield-based inductor.**

I. Introduction

IN 5G millimeter wave communication systems, numerous mm-wave frequency bands have been defined by the Third Generation Partnership Project, including 26.5–29.5 GHz (n257), 24.25–27.5 GHz (n258), and 37–40 GHz (n260).

Research and development regarding multiband or wide-band communication systems has increased in recent years. Although wide-band systems provide increased communication coverage and data throughput, these systems cover both desired and undesired frequencies. These systems cannot be optimized for their main frequency bands, resulting in increased power consumption, decreased RF power efficiency, increased interference with other RF signals, and higher circuit complexity. [1]. Multiband systems have been proposed to replace wide-band systems; such systems would have greater practical utility [2].

In a beamformer IC, the input–output (I/O) of antenna ports is single-ended because of the unbalanced structure of antennas [3], and components in receivers typically use differential topology to reduce noise; therefore, single-input differential-output (SIDO) low-noise amplifiers (LNAs) [4], [5], [6], [7], [8], [9], [10] have been used to connect antennas and differential components in communication systems [10]. However, designing an LNA with simultaneous multiband and SIDO is challenging.

Various multiband LNAs have been described [6], [11], [12], [13], [14], [15], including switched and concurrent multiband LNAs. On the multiband LNA circuit, the input-matching network always uses a fixed single- or wide-band design because switching the input-matching network may cause additional switching losses, increasing noise [13]. Wang et al. [11] used a varactor-based tunable network (VTN) on interstage-matching networks to devise a switched multiband LNA. Nawaz and Albrecht [12] used a transistor to switch the output-matching network, producing a switched multiband LNA. However, the input-matching network of both designs was optimized for only one frequency band; thus, the LNAs had poor input reflection coefficients at other frequency bands. In [13], a substrate-shield inductor (SSI) and switched capacitors on the interstage- and output-matching networks were applied to implement a switched multiband LNA; the input-matching network was divided into three paths for different bands to achieve an improved input reflection coefficient. However, the area of the input-matching network was excessively large, and the three RF input ports were difficult to integrate into a system. In [21] and [22], the SSIs are integrated with switching devices. They were used to implement variable gain LNA [21] and a frequency-reconfigurable power amplifier [22]. Liang et al. [14] used a coupling transformer wide-band design on an input-matching network; transistors were used to switch the interstage- and output-matching networks to achieve a switched multiband. However, a wide-band coupling transformer design cannot be optimized for the main frequency band due to resulting increases in average noise. Agarwal et al. [6] used transformer feedback, and Lee and Nguyen [15] used *LC* filter feedback on a matching network to achieve a concurrent multiband; however, as for wide-band LNAs, these systems could not be optimized in the main frequency band. In differential systems, the aforementioned single-ended components require a larger balun area. Therefore, a multiband SIDO LNA is an attractive research topic.

In this letter, a frequency-reconfigurable SIDO LNA for the two frequency bands of 24.25–29.5 GHz (n257 and n258), and 37–40 GHz (n260) is proposed. This LNA is the first

Manuscript received 2 March 2023; revised 23 May 2023; accepted 15 June 2023. Date of publication 3 July 2023; date of current version 6 September 2023. This work was supported in part by the Center for mmWave Smart Radar Systems and Technologies of Taiwan under the Featured Areas Research Center Program within the framework of the Higher Education Sprout Project by the Ministry of Education of Taiwan; in part by the Qualcomm Project; and in part by the Ministry of Science and Technology (MOST), Taiwan, under Grant 111-2223-E-A49-003-MY3, Grant 109-2221-E-009-124-MY3, Grant 112-2218-E-110-002, and Grant 112-2218-E-002-031. *(Corresponding author: Zuo-Min Tsai.)*

Hao-Hsuan Chen is with the Advanced Institute of Manufacturing with High-Tech Innovations, National Chung Cheng University, Chiayi 62102, Taiwan.

Zuo-Min Tsai is with the Institute of Communications Engineering, College of Electrical and Computer Engineering, and the Center for mmWave Smart Radar Systems and Technologies, National Yang Ming Chiao Tung University, Hsinchu 30050, Taiwan (e-mail: zuomintsai@gmail.com).

Color versions of one or more figures in this letter are available at https://doi.org/10.1109/LMWT.2023.3288625.

Digital Object Identifier 10.1109/LMWT.2023.3288625

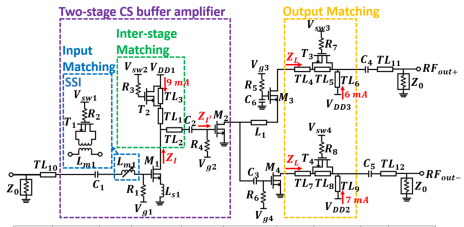

M_1	36 μm	$T_{1,4}$	40 μm	L_{s1}	70 pH	TL_3	300 μm	TL_7	310 μm
$M_{2,3}$	24 μm	C_{1-5}	1.27 pF	L_1	70 μm	TL_4	310 μm	TL_8	390 μm
M_4	28 μm	C_6	0.47 pF	TL_1	330 μm	TL_5	420 μm	TL_9	370 μm
$T_{1,2}$	192 μm	L_{m1}	507 pH	TL_2	295 μm	TL_6	400 μm	R_{1-8}	3.3 kΩ
$V_{DD1,2}$	1 V	V_{DD3}	2 V	V_{sw1}	0/1 V	$V_{sw2,4}$	0/2 V	V_{sw3}	1/3 V
$V_{g1,2,4}$	0.6 V	V_{g3}	1.6 V	TL_{10-12}	50Ω Low Loss Transmission Line				

Fig. 1. Schematic and the design parameters of the proposed frequency-reconfigurable LNA.

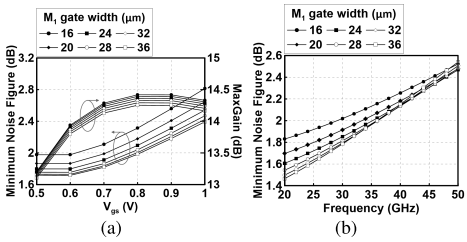

(a) (b)

Fig. 2. (a) Minimum NF, G_{max}, and V_{gs} for various M_1 gate widths at 28 GHz. (b) Minimum NF for various M_1 gate widths.

to achieve a frequency-reconfigurable input-matching network by using an SSI on CMOS 65 nm for 5G communication in n257, n258, and n260 bands. The LNA uses an SSI instead of a single-band or wide-band input-matching network because the tunable inductance of an SSI can enable a superior input reflection coefficient in different frequency bands and lower the switch losses compared with the aforementioned methods. With both tunable interstage- and output-matching networks, the LNA can switch frequency bands and convert single-ended signals to differential signals simultaneously.

II. Circuit Design

The schematic and the design parameters of the proposed frequency-reconfigurable LNA are presented in Fig. 1. This proposed LNA comprises a two-stage common-source (CS) buffer amplifier (M_1 and M_2), a common-gate (CG) amplifier (M_3), a CS amplifier (M_4), and a phase compensation line (L_1). The output ports of the amplifiers M_3 and M_4 are assigned to the differential output signals RFout+ and RFout–. At low frequencies, CG (M_3) and CS (M_4) devices have gains with equal magnitudes and opposite signs. However, at high frequencies, the reactance and parasitic effects of the transistor influence both gain magnitude and phase [10]. Therefore, the common-mode rejection ratio [10] was adopted to determine the optimal ratio of M_3 and M_4 with the phase compensation line L_1.

In LNA design, the first-stage CS device (M_1), source degeneration inductor (L_{s1}), and input inductor (L_{m1}) contribute to the noise. The L_{s1} determines the size selection of M_1 [17], [18], in which the channel noise dominates the noise of the LNA; optimal design parameters of M_1 and L_{s1} for 28 and 39 GHz must be determined for this multiband design. The biasing condition (V_{gs}) and gate width of M_1 versus the minimum NF (NFmin) and maximum transducer gain (G_{max}) at 28 GHz are presented in Fig. 2(a); the performance at 39 GHz is similar to that at 28 GHz. The drain current (I_D) was selected as 50% of $I_{D(peak)}$ (drain current with maximum G_{max}) because of the trade-off between G_{max} and NFmin. Therefore, V_{gs} can be determined to be 0.6 V. For $V_{gs} = 0.6$ V, the frequency responses of NFmin with various M_1 gate widths

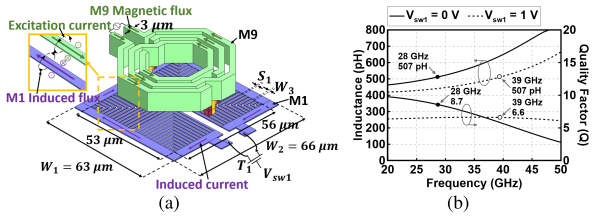

(a) (b)

Fig. 3. (a) Layout and (b) simulated results for the SSI.

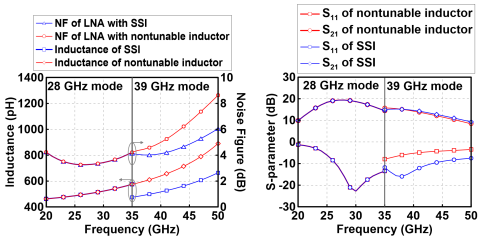

(a) (b)

Fig. 4. (a) NF and (b) S-parameter of an LNA with a nontunable inductor and SSI.

are presented in Fig. 2(b). An M_1 gate width of 2 × 18 μm (36 μm) was selected to minimize NFmin at both 28 and 39 GHz. The input impedance formula Z_{in} in (1) [17] was used to reveal that L_{s1} of 70 pH causes the real part of Z_{in} to be approximately 50 Ω. L_{m1} is selected next to ensure that the imaginary part of the input impedance is close to zero. Because of the parasitic capacitance of the transistor, the optimal L_{m1} for 28 and 39 GHz differ. Therefore, a single fixed inductance value for L_{m1} cannot be optimal for operation frequencies of both 28 and 39 GHz. Insertion loss of the input inductor (L_{m1}) also affects the NF; therefore, the loss of the inductor must be low at both frequency bands. Hence, a switchable SSI was used to switch the inductance, meeting the requirements for both operation frequencies. The SSI has a low insertion loss and wide bandwidth, respectively, [16]

$$Z_{in} = s(L_{m1} + L_{s1}) + \frac{1}{sC_{gs1}} + \left(\frac{g_{m1}}{C_{gs1}}\right)L_{s1}. \quad (1)$$

Fig. 3(a) presents the layout of the SSI. The SSI was fabricated using a 65-nm 1P9M CMOS process. The top metal (M_9) was used for the inductor (L_{m1}), and the bottom metal (M_1) was used for the metal grid structure. The metal grid structure is connected to a transistor (T_1), which operates in passive mode and acts as a switch. The control voltage (V_{sw1}) is used to turn T_1 on and off. When $V_{sw1} = 1$ V ($V_{gs} = 1$ V, 39-GHz mode), the metal grid is a closed loop structure, and the induced current in M_1 produces a magnetic flux, removing some of the magnetic flux of the M_9 inductor. Consequently, the equivalence inductance of L_{m1} is reduced. The tuning range of the SSI is dominated by coupling between the inductor and the metal grid structure; this coupling can be adjusted by modifying the size of the metal grid structure ($W_1 \times W_2$). The metal width W_3 and spacing S_1 are minor parameters that can be used for fine adjustments of performance. Fig. 3(b) presents the simulation results for an SSI. The SSI inductance can be tuned between 507 pH ($Q = 8.7$) at 28 GHz ($V_{sw1} = 0$ V) and 507 pH ($Q = 6.6$) at 39 GHz ($V_{sw1} = 1$ V). Hence, the inductance can be tuned from 632 to 507 pH at 39 GHz ($\Delta L \approx 25\%$). The Q value of the SSI can be increased at high frequencies (39 GHz).

Fig. 4(a) and (b) presents the NF and S-parameters of an LNA with a conventional nontunable spiral inductor (optimized for 28 GHz) and the proposed LNA with an SSI at 28 and 39 GHz. Generally, the inductance of the nontunable

TABLE I
PERFORMANCE COMPARISON OF STATE-OF-THE-ART MULTIBAND LNAS

Ref.	Process	Center Freq. (GHz)	BW_{3dB} (GHz)	Gain (S_{21}/S_{31}) (dB)	NF[a] (NF_{21}/NF_{31}) (dB)	IP_{1dB} ($IP_{1dB,21}$/$IP_{1dB,31}$) (dBm)	IIP_3 ($IIP_{3,21}$/$IIP_{3,31}$) (dBm)	Gain Imbalance (dB)	Phase Imbalance (deg)	S_{11} (dB)	Pdc (mW)	Size (mm^2)	FoM1	FoM2
[1][2,4]	180-nm SiGe	44	8.2	18.9	5.65	–	–13.6	–	–	–8[c]	36.9	0.435	0.75	0.032
		60	9.3	18.7	5.76	–	–13.9	–	–	–7[c]	36.9	0.435	0.78	0.031
[6][1,4]	180-nm SiGe	21.5	7.5	15.7/16.6(19.2[d])	4.3/4.0	–24.3/–23.4	–14.9/–14.1	0.9	0.5	–8	73.8	0.69	0.61[b]	0.02[b]
		36	12.6	15.7/16.7(19.2[d])	4.3/4.2	–25.8/–26.9	–16.8/–16.1	1	10.4	–9	73.8	0.69	0.95[b]	0.2[b]
[11][2,3]	0.1-μm GaAs	28	1.6	25.1	2.4	–18.3	–8.8	–	–	–6[c]	74	1.6	1.51	0.2
		39	3	27.7	2.8	–17	–8.5	–	–	–5[c]	74	1.6	1.09	0.15
[12][2,3]	130-nm SiGe	28	5[c]	16.2	2.8	-12	–	–	–	–15[c]	8.2	0.1	4.34	–
		60	8[c]	15	3.35	-7	–	–	–	–7[c]	21	0.1	1.84	–
[19][2,4]	65-nm CMOS	28	1.1	18.1	3.1	-21.1	–	–	–	–11[c]	10.2	0.16	0.83	–
		39	2.7	18.4	3.8	-21.9	–	–	–	–12[c]	10.2	0.16	1.57	–
[20][2,3]	65-nm CMOS	28.5	4.8	11.1	3.5	-10.5	–	–	–	–15[c]	16.8	0.12	0.82	–
		38	9.4	8.5	4	-6.6	–	–	–	–10[c]	16.8	0.12	1	–
This Work[1,3]	65-nm CMOS	28	9	17.2/16.9(20.1[d])	2.8/3	–13.6/–15.6	–4/–6	0.3	5.4	–25	28.5	0.157	3.52[b]	1.4[b]
		39	16	12.1/11.9(14.9[d])	4.4/4.7	–11/–11	–2/–2	0.2	6	–13	28.5	0.157	1.77[b]	1.12[b]

[1]SIDO LNA, [2]Single-ended LNA, [3]Switching multiband LNA, [4]Concurrent multiband LNA, [a]NF of center frequency, [b]Calculated from differential gain; minimal NF and maximal IIP_3, [c]Estimated; [d]Differential. $\text{FoM1} = \frac{\text{Gain[lin.]} \times \text{BW[GHz]}}{(\text{NF[lin.]}-1) \times P_{dc}\text{[mW]}}$ $\text{FoM2} = \frac{\text{Gain[lin.]} \times \text{BW[GHz]} \times \text{IIP}_3\text{[mW]}}{(\text{NF[lin.]}-1) \times P_{dc}\text{[mW]}}$

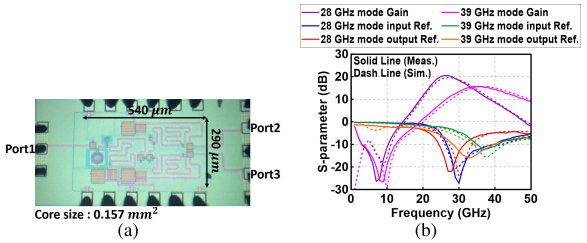

(a) (b)

Fig. 5. (a) Photograph of the SIDO LNA. (b) Measured and simulated results for the *S*-parameter of the SIDO at 28- and 39-GHz mode.

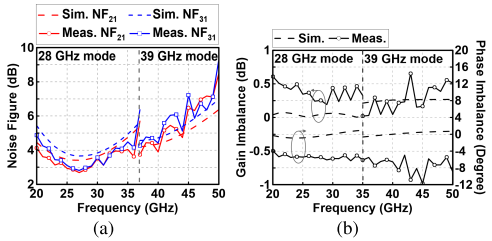

(a) (b)

Fig. 6. (a) Measured and simulated results for single-ended input to single-ended output noise figure, and (b) gain and phase imbalance at 28- and 39-GHz mode.

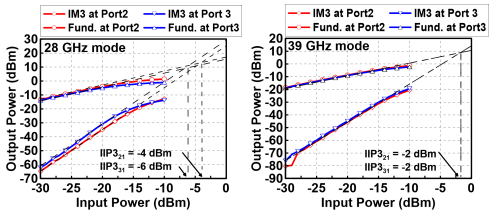

(a) (b)

Fig. 7. Measured power performances of the single-end input to single-ended output in (a) 28-GHz mode and (b) 39-GHz mode.

spiral inductor increases at high frequencies. Therefore, the NF and input reflection coefficient of the LNA with a nontunable spiral inductor degrade at high frequencies. By contrast, the switchable SSI can switch the matching network to optimize its inductance for high-frequency signals, improving the NF from 4.77 to 4.05 dB and the input reflection coefficient from −5.6 to −15 dB at 39 GHz. The LNA optimized for 39 GHz with a nontunable inductor exhibits worse NF and input reflection coefficient compared to the SSI in the low band (28 GHz).

As presented in Fig. 1, the interstage- and output-matching networks were designed by using shunt and series transmission lines. The control voltage $V_{sw2\sim4}$ is used to switch on $T_{2\sim4}$ in order to switch the length of transmission lines. By switching the length of the shunt transmission line, the input impedance ($Z_{I'}$) of M_2 is matched to the $\Gamma_{opt}(Z_I)$ of M_1 at 28/39 GHz. By switching the length of series transmission lines, the output load (Z_0) is matched to the $\Gamma_{opt}(Z_L)$ of M_3 and M_4 at 28/39 GHz. Because the loss of switching devices directly increases the loss of frequency reconfigurable transmission lines, this switching technique only applied on the interstage- and output-matching networks. Hence, with the frequency-reconfigurable SSI, a tunable interstage, and output-matching networks, a multiband single-end-in differential-out LNA can be achieved.

III. MEASUREMENT

A photograph of the SIDO LNA chip is presented in Fig. 5(a). The core area has a size of 0.54 × 0.29 mm. The measured and simulated *S*-parameters of the single-to-differential are presented in Fig. 5(b). The *S*-parameters of single-ended input to differential output are combined with the *S*-parameter of single-ended input to single-ended output (S_{21} and S_{31}). The gains at 28 and 39 GHz, respectively, were 20.1 and 14.9 dB. The 3-dB bandwidths were 9 GHz in the 23–32-GHz band and 16 GHz in the 29–45-GHz band. The measured NFs from 20 to 35 GHz were less than 4 dB; those from 37 to 44 GHz were less than 6 dB, as presented in Fig. 6(a). The gain imbalances were 0.3 and 0.2 dB at 28 and 39 GHz, respectively, and the phase imbalances were both less than 6° [see Fig. 6(b)]. The $IP_{1dB,21}$ and $IP_{1dB,31}$ were −13.6 and −15.6 dBm, respectively, at 28 GHz and −11 and −11 dBm, respectively, at 39 GHz. The $IIP_{3,21}$ and $IIP_{3,31}$ were −4 and −6 dBm at 28 GHz, and −2 and −2 dBm at 39 GHz, as presented in Fig. 7(a) and (b). These measurements are in good agreement with the simulated results. A comparison of the proposed SIDO LNA and those of other studies is presented in Table I. The comparison reveals that the proposed LNA has a high gain, a good input reflection coefficient, a small core size, and a high figure of merit (FoM).

IV. CONCLUSION

The proposed frequency-reconfigurable SIDO LNA is applicable for *K*- and *Ka*-band 5G communication systems and can be produced using the TSMC 65-nm CMOS process. The input reflection coefficient can be optimized for the main frequency, and the switched band range can be defined by the designer. The measurement results indicate that the performance of the proposed LNA is comparable to that of others' LNAs. It also has a small core size of 0.157 mm^2. FoM1 and FoM2 at 28 GHz were 3.52 and 1.4; those at 39 GHz were 1.77 and 1.12. Hence, the proposed LNA is suitable for *K*- and *Ka*-band 5G communications applications.

REFERENCES

[1] D. Lee and C. Nguyen, "Dual Q/V-band SiGe BiCMOS low noise amplifiers using Q-enhanced metamaterial transmission lines," *IEEE Trans. Circuits Syst. II, Exp. Briefs*, vol. 68, no. 3, pp. 898–902, Mar. 2021.

[2] Y. Lin and Z. Tsai, "Frequency-reconfigurable phase shifter based on a 65-nm CMOS process for 5G applications," *IEEE Trans. Circuits Syst. II, Exp. Briefs*, vol. 68, no. 8, pp. 2825–2829, Aug. 2021.

[3] B. Liu, G. Chen, and Y. Chen, "A 24-GHz single-to-differential LNA for K-band receiver applications," in *Proc. IEEE Int. Conf. Microw. Millim. Wave Technol. (ICMMT)*, vol. 1, Jun. 2016, pp. 511–513.

[4] H. Chen, C. Wu, Y. Lin, and J. Y. Liu, "A K-band area-saving Marchand balun integrated with low-noise amplifier in 0.18-μm CMOS," in *Proc. IEEE Asia Pacific Microw. Conf. (APMC)*, Kuala Lumpur, Malaysia, Nov. 2017, pp. 1196–1199.

[5] S. Raghu, S. Sunny, and P. Duraiswamy, "High performance three-stage 30 GHz CMOS single-to-differential LNA," in *Proc. 15th IEEE India Council Int. Conf. (INDICON)*, Coimbatore, India, Dec. 2018, pp. 1–4.

[6] J. Lee and C. Nguyen, "A $K-/Ka$-band concurrent dual-band single-ended input to differential output low-noise amplifier employing a novel transformer feedback dual-band load," *IEEE Trans. Circuits Syst. I, Reg. Papers*, vol. 65, no. 9, pp. 2679–2690, Sep. 2018.

[7] C. Geha, C. Nguyen, and J. Silva-Martinez, "A wideband low-power-consumption 22–32.5-GHz 0.18-μm BiCMOS active balun-LNA with IM2 cancellation using a transformer-coupled cascode-cascade topology," *IEEE Trans. Microw. Theory Techn.*, vol. 65, no. 2, pp. 536–547, Feb. 2017.

[8] L. Gao and G. M. Rebeiz, "A 22–44-GHz phased-array receive beamformer in 45-nm CMOS SOI for 5G applications with 3–3.6-dB NF," *IEEE Trans. Microw. Theory Techn.*, vol. 68, no. 11, pp. 4765–4774, Nov. 2020.

[9] Y. Hu and T. Chi, "A 27–46-GHz low-noise amplifier with dual-resonant input matching and a transformer-based broadband output network," *IEEE Microw. Wireless Compon. Lett.*, vol. 31, no. 6, pp. 725–728, Jun. 2021.

[10] H.-H. Chen, W.-C. Cheng, C.-H. Hsieh, and Z.-M. Tsai, "Design and analysis of high-gain and compact single-input differential-output low noise amplifier for 5G applications," *IEEE Microw. Wireless Compon. Lett.*, vol. 32, no. 6, pp. 535–538, Jun. 2022.

[11] Z. Wang et al., "A ka-band switchable LNA with 2.4-dB NF employing a varactor-based tunable network," *IEEE Microw. Wireless Compon. Lett.*, vol. 31, no. 4, pp. 385–388, Apr. 2021.

[12] A. A. Nawaz, J. D. Albrecht, and A. Ç. Ulusoy, "A Ka/V band-switchable LNA with 2.8/3.4 dB noise figure," *IEEE Microw. Wireless Compon. Lett.*, vol. 29, no. 10, pp. 662–664, Oct. 2019.

[13] R. A. Shaheen, T. Rahkonen, and A. Pärssinen, "Millimeter-wave frequency reconfigurable low noise amplifiers for 5G," *IEEE Trans. Circuits Syst. II, Exp. Briefs.*, vol. 68, no. 2, pp. 642–646, Feb. 2021.

[14] C. Liang et al., "A tri (K/Ka/V)-band monolithic CMOS low noise amplifier with shared signal path and variable gains," in *IEEE MTT-S Int. Microw. Symp. Dig.*, Aug. 2020, pp. 333–336.

[15] J. Lee and C. Nguyen, "A concurrent tri-band low-noise amplifier with a novel tri-band load resonator employing feedback notches," *IEEE Trans. Microw. Theory Techn.*, vol. 61, no. 12, pp. 4195–4208, Dec. 2013.

[16] P. Agarwal et al., "Switched substrate-shield-based low-loss CMOS inductors for wide tuning range VCOs," *IEEE Trans. Microw. Theory Techn.*, vol. 65, no. 8, pp. 2964–2976, Aug. 2017.

[17] K.-J. Sun, Z.-M. Tsai, K.-Y. Lin, and H. Wang, "A noise optimization formulation for CMOS low-noise amplifiers with on-chip low-Q inductors," *IEEE Trans. Microw. Theory Techn.*, vol. 54, no. 4, pp. 1554–1560, Jun. 2006.

[18] D. K. Shaeffer and T. H. Lee, "A 1.5-V, 1.5-GHz CMOS low noise amplifier," *IEEE J. Solid-State Circuits.*, vol. SSC-32, no. 5, p. 745–759, May 1997.

[19] J. Liu, S. Liu, Y. Gao, X. Liu, and Z. Zhu, "A 28-/39-GHz dual-band CMOS LNA with shunt-series transformer feedback," *IEEE Microw. Wireless Technol. Lett.*, vol. 33, no. 1, pp. 51–54, Jan. 2023.

[20] S. Lee and S. Hong, "Frequency-reconfigurable dual-band low-noise amplifier with interstage gm-boosting for millimeter-wave 5G communication," *IEEE Microw. Wireless Technol. Lett.*, vol. 33, no. 4, pp. 463–466, Apr. 2023.

[21] S. N. Ali, M. A. Hoque, S. Gopal, M. Chahardori, M. A. Mokri, and D. Heo, "A continually-stepped variable-gain LNA in 65-nm CMOS enabled by a tunable-transformer for mm-Wave 5G communications," in *IEEE MTT-S Int. Microw. Symp. Dig.*, Jun. 2019, pp. 926–929.

[22] S. N. Ali, P. Agarwal, J. Baylon, and D. Heo, "Reconfigurable high efficiency power amplifier with tunable coupling coefficient based transformer for 5G applications," in *IEEE MTT-S Int. Microw. Symp. Dig.*, Jun. 2017, pp. 1177–1180.